PAPER • **OPEN ACCESS**

Mesoscale-coupled Large Eddy Simulation for Wind Resource Assessment

To cite this article: Rupert Storey and Rene Rauffus 2024 *J. Phys.: Conf. Ser.* **2767** 052040

Journal of Physics: Conference Series **2767** (2024) 052040 doi:10.1088/1742-6596/2767/5/052040

Mesoscale-coupled Large Eddy Simulation for Wind Resource Assessment

Rupert Storey[1] **and Rene Rauffus**[2]
[1] GE Vernova, Onshore Wind, Berlin
[2] GE Vernova, Onshore Wind, Barcelona

E-mail: rupert.storey@ge.com

Abstract. Turbulence, a key driver of wind turbine loads, is central in the assessment of turbine suitability and performance, and consequently impacts the expected energy production of a wind farm. Conventional flow modeling methods for wind resource assessment (WRA) typically lack the ability to resolve turbulence due to key simplifications in their formulation. This work applies Large Eddy Simulation (LES) to address these limitations and deliver high-fidelity wind condition predictions at 24 wind farm sites. The model includes recently improved boundary conditions to downscale information from global weather models via a mesoscale layer. Validation of the model is presented through comparison to over 100 years of measurements, with comparison of the time-series, distributions and spectra. Validation results indicate excellent performance of the model for key flow quantities including wind speed, turbulence and direction. Comparison of spectra indicates a significant improvement in the representation of the atmospheric energy cascade when compared to previous approaches. The results are significant for wind-farm site assessment as they demonstrate the feasibility of applying accurate LES at a commercial scale. LES also provides a step change in the quality of model predictions through resolving time and site-specific turbulence characteristics. The application of the model for WRA is a step towards improved understanding of the wind resource, as well as an improved suitability assessment process itself.

1. Introduction

Precise characterization of wind conditions is essential for evaluating the feasibility of wind farm projects. Wind speeds on a site determine the energy resource, while turbulence is the main driver of wind turbine loads[1]. Together, these two quantities are central to the assessment of turbine suitability. Uncertainty in these quantities is a key factor in the bias and uncertainty of energy yield analyses[2]. The need to better understand the wind resource and farm-scale wind interactions has been highlighted one of the grand challenges of wind energy[3].

Conventional modelling methods for wind resource assessment (WRA) typically lack the capacity to resolve turbulence due to simplifications in their formulation. Limited turbulence information leaves the WRA process heavily dependent on met-mast measurements to characterise the site. Although measurements offer low local uncertainty, they are constrained in both spatial and temporal coverage, as well as measurement height.

Large Eddy Simulation (LES) provides a solution to augment measurements and improve the predictions of site-specific wind conditions. The method emphasises a physics-driven approach; by removing modelling assumptions, especially around turbulence, LES provides a fundamentally different view of the wind resource compared to traditional approaches. LES naturally yields

time-correlated results, providing downstream analyses with a more realistic portrayal of dynamic wind conditions. The resolution of time and the elimination of simplifications also open avenues for incorporating additional physics, such as wind-turbine models for wake and load predictions, as demonstrated in prior research [4, 5, 6, 7].

While providing high fidelity, LES models have historically been prohibitively expensive and time-consuming to apply in WRA due the large spatial- and temporal-scale requirements. The development of GPU resident software and improved computing resources however, have effectively removed these constraints. With cloud computing resources readily available, computation times and data storage issues can be effectively managed. Another hurdle to high-fidelity simulations are the complex boundary conditions required for accurate and well-posed representation of the flow. Previous work has highlighted challenges with "down-scaling" information from global weather models to meso- and micro-scales [8, 9, 10]. In the case of LES, the modelling framework must deal with the transition of spatial and temporal scales as well as the switch from parameterised to resolved turbulence.

In this work we apply LES with boundary conditions generated through physical-dynamic coupling with a mesoscale model. This allows the framework to navigate the "Terra Incognita"[11] and to accurately capture the turbulent energy cascade in the atmosphere. The model itself and its application are described below, along with validation cases demonstrating the accuracy of the approach and improvement of results compared to previous validation efforts.

2. Methodology

2.1. Aspire

The atmospheric LES model, *ASPIRE*, is developed by *Whiffle* in the Netherlands. The framework has evolved from a meteorological formulation with an anelastic formulation for buoyancy and the inclusion of transport terms for temperature and humidity. Terrain is represented using an immersed boundary technique, with the land-air interface modelled in detail including time and location dependent heat and moisture fluxes. A micro-physics scheme is employed, along with a radiation scheme capturing solar and terrestrial fluxes. This allows the model to resolve atmospheric phenomena such as stability, convection and cloud formation - key to the accurate representation of the wind.

Several global datasets are used as inputs to the model and are prepared in a pre-processing step. The orography is taken from the recent, 30m resolution Ensemble Digital Terrain model [12]. The ESA World-cover land-use map [13] is used to characterise the surface by setting a land-use dependent surface roughness length (z_0), as well as parameters for the TESSEL surface scheme, similar to that used in the global weather model by ECMWF[14]. The *ASPIRE* formulation has been described in detail in previously, along with validation of its use in wind resource and wake modelling[4, 5, 8, 15, 16].

In prior work[8], the LES used periodic boundary conditions and represented synoptic scale changes in weather through dynamic tendencies derived from ERA5[14]. The periodic conditions simplified the model formulation and allowed for turbulence to be recycled. In the new setting, the LES is driven by a mesoscale model at its boundaries, which itself is forced with lateral boundary conditions from ERA5. Figure 1 shows the new nested setup of the simulations. This switch represents three major changes; firstly the removal of the periodic conditions for more physical open boundary conditions, secondly, the introduction of the mesoscale intermediate domain to resolve mesoscale structures, and third, the inclusion of turbulence perturbations to switch from modelled to resolved turbulence at the interface of the meso- and LES simulations. These perturbations are temporally and spatially dependent to be consistent with the mesoscale inflow conditions, and are derived from a concurrent, periodic LES precursor.

The size of the mesoscale domain and meshes were determined through sensitivity studies and represent an effective trade-off between resolution and computational cost. The mesoscale

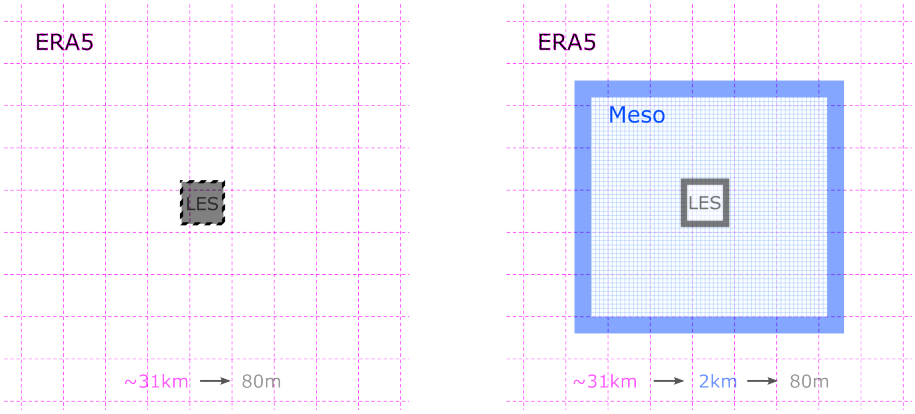

Figure 1: Schematic of the previous pseudo-periodic boundary conditions (left) compared to the new meso-coupled setup (right). Shaded areas (grey and blue) illustrate where boundary conditions are applied. Grid resolutions are also shown for the respective domains.

domain sides measure 256km, while the LES domain sides are 30km to capture typical wind farm sizes. Grid resolutions in the horizontal direction were set to 2km×2km×40m for the meso-domain and 80m×80m×20m for the LES. These ratios ensure each nested domain captures large-scale gradients from its parent. The vertical mesh size is constant in the lower domain to resolve terrain and lower boundary layer gradients. A roughness and stability dependent wall model is employed in the LES which models the velocity profile near the ground.

Both LES and mesoscale models are formulated exclusively for GPU hardware and run simultaneously. This avoids separate models and ensures the simulations are tractable, and cost-effective in a standard WRA process. Simulation days can be fully parallelised, where each day is simulated on a single GPU, taking on average 5 hours to complete. Results are then concatenated to form the final time-series. Simulations therefore require a "spin-up" period for each day to allow flow structures to evolve before recording results. Spin-up periods were set to 12 hours and 2 hours for the meso- and LES domain respectively. For a nominal wind speed of $6ms^{-1}$, the spin-up time allows for the flow to propagate at least 1 complete domain length. Figure 2 shows an example snap-shot of the coupled simulation in a complex mountain pass.

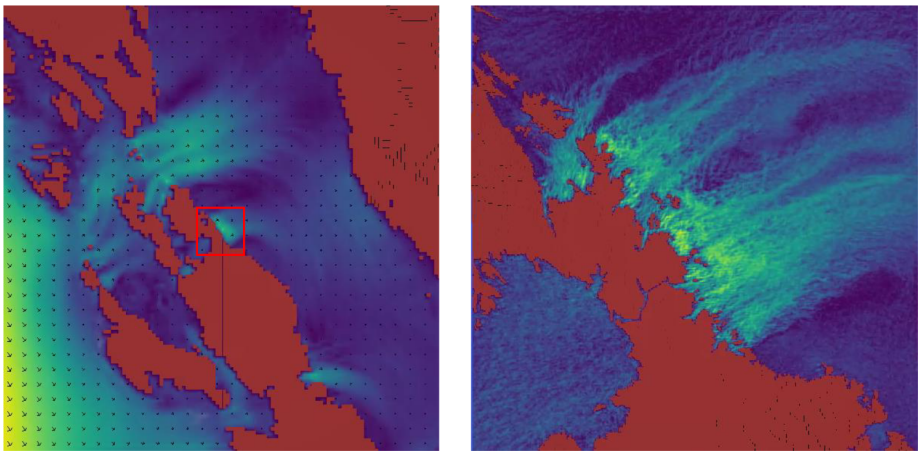

Figure 2: A mesoscale simulation (left) and the nested LES (right) in a complex mountain pass. The flow is visualised on a horizontal plane, intersecting the terrain (shown in red). Regions of high velocity are shown in yellow. The red square shows the nested LES area.

2.2. Validation

2.2.1. Data

Model performance is evaluated over a set of 109 met-masts across 24 sites from a range of climates and terrain complexities. The mast data have been carefully vetted and cleaned for validation purposes. Each site has a varying number of masts ranging 1 to 15 masts, with a typical number of 3 masts per site. Each mast spans roughly 1 year of data, resulting in a validation data-set of over 100 years of 10-min data. The locations of the validation sites are illustrated in Figure 3.

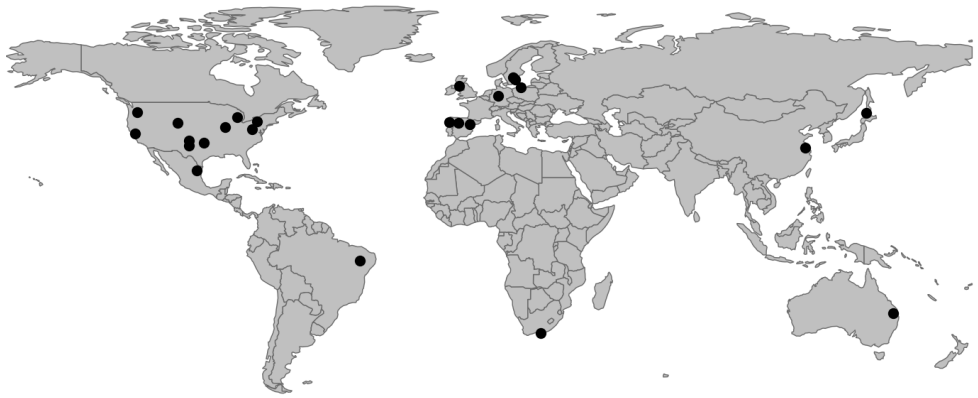

Figure 3: Locations of the 24 validation sites in different parts of the world. These locations cover varied local climates and terrain complexities.

At each site, a simulation is conducted to produce results concurrent with the respective measurement period. Overall, the simulations cover an area of over 22,000km^2 - approximately the size of Slovenia, or the state of New Jersey.

Data were extracted from the model on terrain-following slices and virtual met-mast locations. 10-minute statistics are recorded for horizontal velocity (*vel*), its standard deviation (*std*), and wind direction (*dir*), with sampling every simulation time-step to mimic the met-mast measurement technique. Turbulence is therefore effectively separated into 2 frequency ranges - sub-10 minute frequencies which are resolved by the model are captured in *std*, while velocity fluctuations with period longer than 10 minutes are captured in the *vel* time-series.

2.2.2. Metrics

Two skill metrics, Mean Bias Percentage Error (MBPE) and Mean Absolute Error (MAE) are defined to quantify the error between the model and measurements, described in Eq. 1) and 2). MBPE, indicates whether the model is over-predicting or under-predicting flow quantities on average. For wind direction, the circular mean is taken instead and normalized by the worst possible error, i.e 180°. Due to its normalization feature, MBPE is well-suited for cross-site comparisons, even when climatic conditions vary between sites. While MBPE effectively captures the overall bias of the model, it does not account for phase errors between the model and mast time-series. MAE addresses this limitation by evaluating the mean of the absolute differences between the model and mast at each time sample

$$MBPE = \frac{Mean(model(t)) - Mean(mast(t))}{Mean(mast(t))} \tag{1}$$

$$MAE = \frac{\sum_t^N |model(t) - mast(t)|}{N} \tag{2}$$

In addition to time-series analysis, MAE is employed to evaluate the histograms of wind speed, turbulence, and wind direction, which are commonly used in wind resource assessment. This metric provides the average frequency error for each bin in the histogram. The specific bins chosen for the histograms are $1m/s$, $0.1m/s$ and 20° respectively. To obtain a metric that reflects the typical error at each site, we averaged skill metrics across all masts at a given site, ensuring that sites with more masts are not unduly weighted in the error assessment.

Spectral analysis of the 10-minute velocity signal was also conducted to quantify the effect of the improved simulation boundary conditions on velocity fluctuations with scales with periods larger than 10 minutes. A 1-sided power spectrum was estimated using the discrete Fourier transform of the *vel* signal with results averaged over exponentially increasing bins to remove noise. For a given site, the spectra for both the simulation and measurements were calculated at all masts locations and averaged to aggregate results.

3. Results

Results first focus on validation of the new mesoscale-driven LES versus measurements, with comparisons to the older periodic LES also presented. Aggregated metrics for all sites are shown in Figures 4, 5 and 6. Results demonstrate that simulations are able to accurately assess site characteristics in terms of velocity (*vel*), wind-speed standard-deviation or turbulence (*std*) and wind direction (*dir*), and that the addition of mesoscale information reduces the error between mast-measurements and simulation.

3.1. Skill Metrics

Figure 4 shows aggregated MBPE skill metrics, revealing trends in the model's performance. Generally, the model tends to slightly underestimate wind speeds and overestimate sub 10-minute turbulence, while accurately predicting wind direction. These biases are typically rectified in a downstream calibration process during wind resource assessment, making them easily correctable. However, the more intricate challenge involves minimizing the spread of model error. In this case, we see that the addition of mesoscale information has a positive impact in reducing error spread as quantified by tighter inter-quartile ranges in the Meso-LES results (blue) compared to the Periodic-LES (orange). Notably, wind direction MBPE exhibits outliers at two sites with opposing bidirectional wind roses. These outliers are a statistical artifact, reflecting the metric's limitations when applied to such complex wind roses.

The MAE results, shown in Figure 5, provide further insights, with a median deviation of $1.6m/s$ for wind velocity, $0.31m/s$ for turbulence and 19° for wind direction. The meso-coupled model again shows a marked decrease in error, as well as smaller error spreads. The MAE metric includes phase error, which makes this decrease even more notable as the meso-coupled simulations effectively allow more degrees-of-freedom through the larger range of length-scales that are resolved in the simulation. Outlier results are observed for some flow quantities, although these depend on the site in question as the metric is not normalised. The largest errors in this case are from a single site with a median wind speed close to 10m/s in the main wind directions.

MAE calculated on histograms is shown in Figure 6. These demonstrate the model's capability to accurately predict annual distributions of the local climate variables. On average, the model will predict the histogram bins with an accuracy of around 1% on any given site. This is a strong indication that the model is successfully capturing site-specific trends and phenomena.

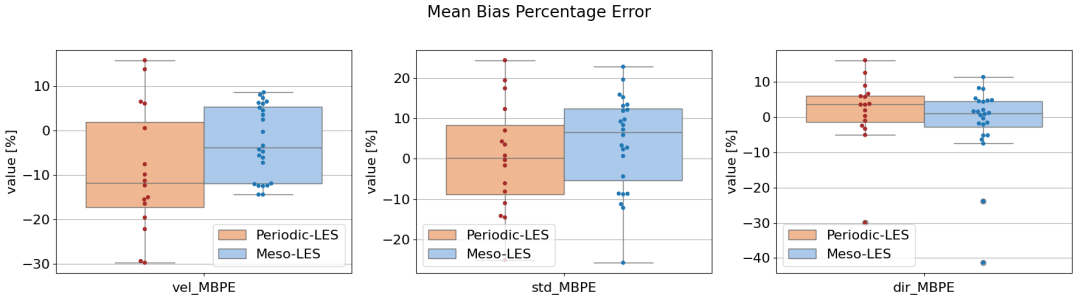

Figure 4: Mean Bias Percentage Errors for all 24 validation sites. From left to right the plots show: wind speed, turbulence, wind direction. Each dot represents the site average over masts at each site. The boxes display the inter-quartile ranges, with whiskers extending to the furthest data point within 1.5 times this range.

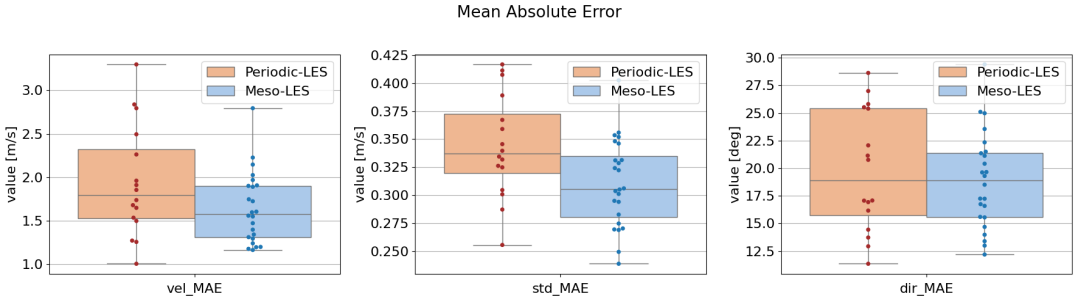

Figure 5: Aggregated Mean Absolute Errors of time-series signals for all 24 validation sites. From left to right the plots show: wind speed, wind-speed standard-deviation, wind direction. Dots represent the site average over masts at each site.

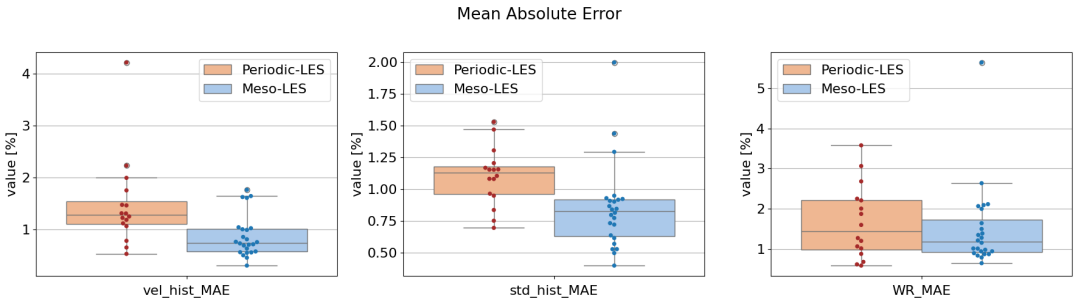

Figure 6: Aggregated Mean Absolute Errors of the wind speed histogram, wind-speed standard-deviation histogram and wind-rose (from left to right) for all 24 validation sites. Dots represent the site average over masts at each site. The bins are $1m/s$, $0.1m/s$ and $20°$ respectively. The boxes display the inter-quartile ranges, with whiskers extending to the furthest data point within 1.5 times this range.

3.2. Site-specific results

The aggregated metrics above summarise the performance of the model overall. At some sites especially, mesoscale flow phenomena have a distinct influence on the results. In this section, we examine a Central American site (site No. 8) which is heavily influenced by large-scale terrain features just outside of the LES domain, but resolved by the mesoscale domain. The site is considered complex, with base elevation differences among the masts of 150m, large elevation

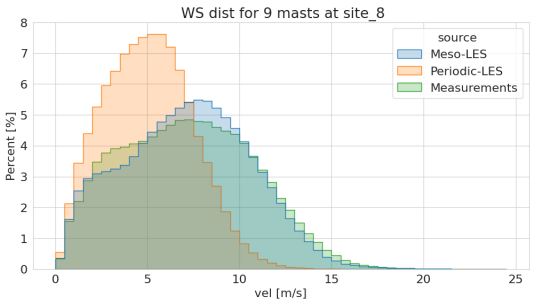

(a) Wind-speed histogram of Site No. 8, comparing the older version of periodic-LES with mesoscale-LES against measurements of 9 masts. Wind speeds are binned with $1m/s$ bins.

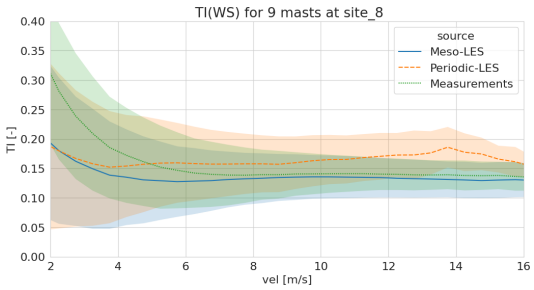

(b) TI-curve of Site No. 8, comparing the older version of periodic-LES with mesoscale-LES against measurements of 9 masts. The solid curves, represent the mean TI of the given $1m/s$ bin. Shaded areas representing the standard deviation of TI in that bin.

Figure 7: Wind-speed histogram and TI-curve

differences over the wider LES domain of over 1000m and maximum gradients of over 30%. The mesoscale domain also recorded elevation differences of over 3000m over its extent.

Figures 7 and 8, illustrate the effect of including the mesoscale layer on wind speed distribution, turbulence versus velocity curve and wind rose. The large-scale terrain at this site drives a speed-up effect with a significant impact on wind speed distribution. The TI curve is also improved over most wind speeds. Some disparity between predictions and measurements is seen for very low-wind speeds. This trend is observed at multiple sites, especially where stable atmospheric conditions are common. It is likely that turbulence scales in these cases fall below the LES filter length and are modelled in the sub-grid model.

In the context of an OEM, where turbine load estimations can dictate the viability of a project, we see a relevant improvement in predictions for wind-speed and TI (Fig 7), which are the main load driving variables. This is particularly true for the "knee" region of typical turbine thrust-curves, $8-10m/s$, where loads tend to be highest, and where model errors can have a significant impact in business decisions. Additionally, the improved wind rose prediction in Figure 8 shows that the model now more accurately captures the dominant wind sectors. This will positively affect wake and blockage modelling and therefore improve load and AEP predictions.

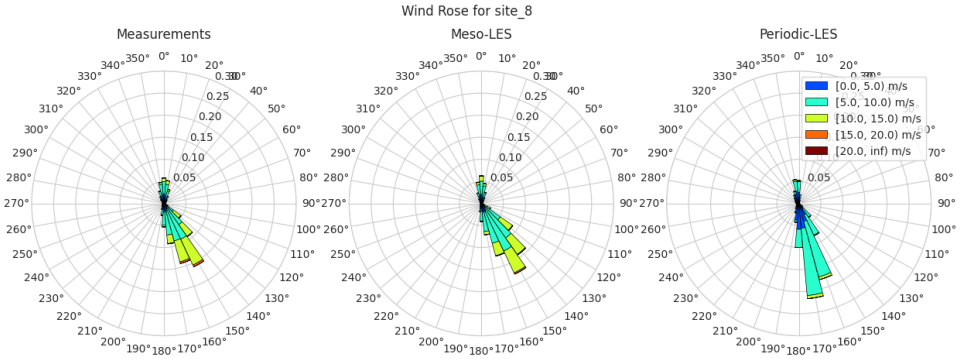

Figure 8: Wind rose comparison at Site No. 8, for the older version of periodic-LES and newer mesoscale-LES against measurements of 9 masts. Wind-speed frequencies are binned in 10° sectors.

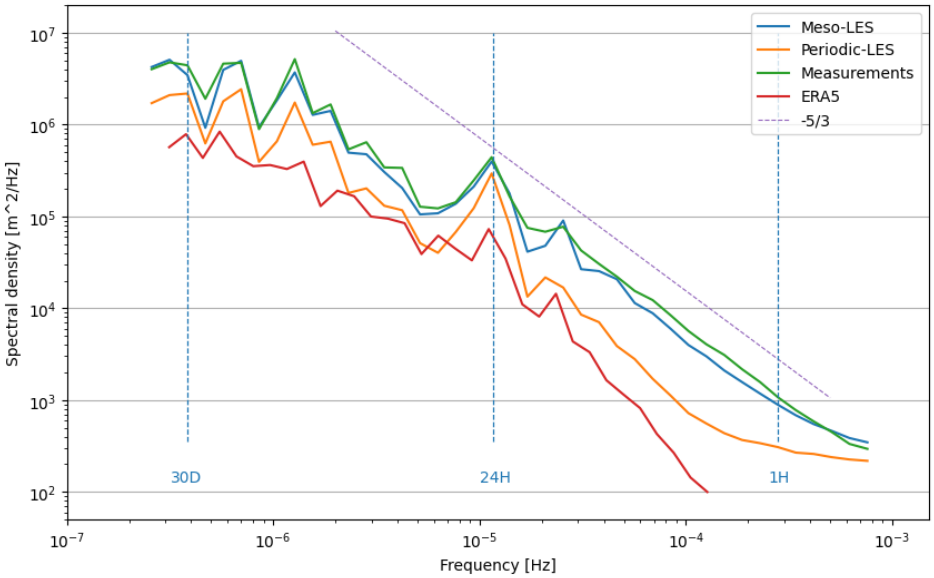

Figure 9: Turbulence spectra aggregated over all masts as Site No. 8 comparing the mesoscale driven LES results to multiple data sources including ECMWF ERA5. The improved boundary conditions show the accurate reproduction of turbulent energy compared to observations.

3.3. Spectra

Figure 9 illustrates the power spectral densities at the same Central American site. A typical peak in energy at the diurnal cycle period of 24 hours is observed for all data sources. A significant gap in energy between observations and ERA5 is shown, especially for frequencies with a period from 2 to 8 hours. This trend is consistent with the large grid size of the model and 1 hour data frequency.

Using the reanalysis data alone to drive the LES simulations with quasi-periodic boundaries also resulted in a marked gap in energy around the mesoscales, peaking around a period of 1.8 hours (1.5×10^{-4}Hz), although this gap reduces at higher frequencies where the LES model can resolve smaller scale fluctuations. The meso-coupled approach shows a significant improvement and correctly reproduces the gradient of the energy cascade in the inertial sub-range when compared to observations. Only small deviations in energy are noted over the entire spectrum. A crossover is noted at a period of around 30 minutes (5×10^{-4}Hz) where the LES starts to predict higher energy than observations. The gradient of the spectrum also starts to deviate from the classical -5/3 gradient described by Kolmogorov. This trend is consistent with the slight over prediction of *std* (sub 10-minute deviations) noted in section 3.1.

4. Discussion

Overall the results show a significant step forward in model performance compared to previous validation efforts. Major changes to the boundary conditions and simulation setup of *ASPIRE* have been shown to have a positive impact on almost all skill metrics.

Some short-comings of the model have been identified such as an increase in bias in *std*, however this is counteracted by a decrease in error-spreads overall, suggesting a generalised increase in model skill and more physically consistent formulation. Results from the spectral analysis were also particularly striking and demonstrated a major step in the quality of time-dependent predictions from the model. Although turbine loads are typically dominated by sub-10-minute scales, larger scale fluctuations are known to feed these smaller scales, and contribute

to long-cycle fatigue loading which for some sites makes up a significant portion of the overall fatigue load. Correctly resolving the power spectrum also has important consequences when predicting extreme wind conditions.

It should be emphasized that the results presented in this work are raw outputs from the model without any input from local measurements. Calibration of flow model outputs with measured time-series data as anchors is standard practice in WRA and will remove the majority of systematic biases in the model results. The intention in this work is to present a transparent view of the underlying modelling capability and its potential to improve standard industry practices.

Further improvements to the model are planned by its developers, including the addition of a dedicated canopy model with global applicability. This will replace the current surface roughness approach with a quadratic drag representation based on forest height and density. The authors also plan to utilise the models extensibility in future work though the inclusion of turbines represented by actuator models for further validation.

In practical terms, the utilization of GPU-native simulation engine enabled full-year high-fidelity simulations in less than 8 hours. Such turn-around times are compatible with industry project timelines, which means that for standard WRA projects, no trade-off is needed between speed and physical fidelity. This computational agility also renders wind simulations tractable for broader applications in wind energy, like coupled wake and machine loads simulations.

5. Conclusions

This work presents the application of the *ASPIRE* LES model with recently improved boundary conditions and the addition of a mesoscale model. The approach down-scales information from synoptic and mesoscales down to the microscale, offering an improved understanding of wind flow across different terrains and climates. This represents a significant step forward in robust and explainable modelling for WRA.

The model was validated against a comprehensive dataset of more than 100 years of measurement data across 24 sites with diverse environmental conditions. A comparison with an older model version which used quasi-periodic boundary conditions demonstrates the contribution of the mesoscale coupling and improved boundary conditions, showing reduced overall errors and narrower error spreads. The model achieves accurate predictions of wind-speed, turbulence, and wind-direction distribution, with errors consistently within 1% per bin.

Significant improvements are observed in sites influenced by strong large-scale weather patterns, showcasing the model's capacity to address complex atmospheric interactions. Spectral analysis confirms the ability of the model to accurately reproduce the distribution of energy in the atmosphere, providing insights into previously unexplored dynamics compared to traditional WRA.

Furthermore, the focus on resolving physics rather than relying on assumptions enhances the interpretability of model results, which simplifies analysis and allows for one-to-one validation with mast measurements. This characteristic also prepares for integration with other engineering models that benefit from time resolved dynamics, contributing to a more comprehensive understanding of not only wind but also turbine interactions and beyond. Full digital-twin wind farms, could one day be powered by such physics informed models to anchor or train tools in the age of data-driven AI.

References

[1] Mücke T, Kleinhans D and Peinke J 2011 *Wind Energy* **14** 301–316 ISSN 1095-4244, 1099-1824
[2] Todd A C, Optis M, Bodini N, Fields M J, Perr-Sauer J, Lee J C Y, Simley E and Hammond R 2022 *Wind Energy* ISSN 1095-4244, 1099-1824
[3] Veers P, Dykes K, Lantz E, Barth S, Bottasso C L, Carlson O, Clifton A, Green J, Green P, Holttinen H, Laird D, Lehtomäki V, Lundquist J K, Manwell J, Marquis M, Meneveau C, Moriarty P, Munduate

X, Muskulus M, Naughton J, Pao L, Paquette J, Peinke J, Robertson A, Rodrigo J S, Sempreviva A M, Smith J C, Tuohy A and Wiser R 2019 *Science* **366** eaau2027 ISSN 0036-8075 (*Preprint* `https://www.science.org/doi/pdf/10.1126/science.aau2027`)

[4] Baas P and Verzijlbergh R 2022 The impact of wakes from neighboring wind farms on the production of the IJmuiden ver wind farm zone Tech. rep. Whiffle

[5] Baas P, Verzijlbergh R, van Dorp P and Jonker H 2023 *Wind Energy Sci.* **8** 787–805 ISSN 2366-7443, 2366-7451

[6] Storey R 2014 *Large Eddy Simulation of Dynamically Controlled Wind Turbine Arrays* Ph.D. thesis University of Auckland

[7] Storey R C, Cater J E and Norris S E 2016 *Renewable Energy* **95** 31–42 ISSN 0960-1481

[8] Kantharaju J, Storey R, Julian A, Delaunay F and Michaud D 2023 *J. Phys. Conf. Ser.* **2507** 012015 ISSN 1742-6588, 1742-6596

[9] Sanz Rodrigo J, Chávez Arroyo R A, Moriarty P, Churchfield M, Kosović B, Réthoré P E, Hansen K S, Hahmann A, Mirocha J D and Rife D 2017 *Wiley Interdiscip. Rev. Energy Environ.* **6** e214 ISSN 2041-8396, 2041-840X

[10] van Stratum B J H, van Heerwaarden C C and Vilà-Guerau de Arellano J 2023 *J. Adv. Model. Earth Syst.* **15** ISSN 1942-2466

[11] Wyngaard J C 2004 *J. Atmos. Sci.* **61** 1816–1826 ISSN 0022-4928, 1520-0469

[12] Ho Y F, Hengl T and Parente L 2023 Ensemble digital terrain model (EDTM) of the world

[13] Zanaga D, Van De Kerchove R, Daems D, De Keersmaecker W, Brockmann C, Kirches G, Wevers J, Cartus O, Santoro M, Fritz S, Lesiv M, Herold M, Tsendbazar N E, Xu P, Ramoino F and Arino O 2021 ESA WorldCover 10 m 2021 v200

[14] Muñoz Sabater J 2019 ERA5-Land hourly data from 1950 to present. copernicus climate change service (C3S) climate data store (CDS)

[15] Heus T, van Heerwaarden C C, Jonker H J J, Pier Siebesma A, Axelsen S, van den Dries K, Geoffroy O, Moene A F, Pino D, de Roode S R and Vilà-Guerau de Arellano J 2010 *Geosci. Model Dev.* **3** 415–444 ISSN 1991-959X, 1991-9603

[16] Schalkwijk J, Jonker H J J, Pier Siebesma A and Bosveld F C 2015 *Mon. Weather Rev.* **143** 828–844 ISSN 0027-0644, 1520-0493